# Range Data Matching for Object Recognition Using Singular Value Decomposition

**Takeshi NISHIDA, Seiichiro YAMADA,**
**Ayako EGUCHI, Yasuhiro FUCHIKAWA and Shuichi KUROGI**
**Department of Control Engineering, Kyushu Institute of Technology,**
**1-1 Sensui Tobata, Kitakyushu, Fukuoka 804-8550, Japan**

## ABSTRACT

In this paper, we propose a 3-D object recognition method for range datasets obtained by a LRF (Laser Rangefinder). Since the resolution of the measured data from the LRF changes according to the distance from the LRF to the target object, the memorized template dataset and the measurement dataset can hardly be corresponded each other in general, and then the computational cost of matching the datasets is very high and it is difficult to execute the matching stably. To overcome these problems, we propose an algorithm using singular value decomposition (SVD) for identifying 3-D affine transformation between the memorized and the measured datasets with high speed and stability Moreover, through numerical simulations and actual experiments, we demonstrate that our method is able to achieve stable and robust recognition of range datasets.

**Keywords:** Computer vision, Laser Rangefinder, Estimating 3-D affine transformation, 3-D Pattern Matching, Singular Value Decomposition.

## 1. INTRODUCTION

Recently, in computer vision applications, the object recognition methods for 3-D datasets obtained by a LRF (Laser Rangefinder) (for example [1], [2]) are proposed [3], [4]. The global and local shape matching metrics for free-from curves and surfaces as well as point sets were described in these researches. The problem is formalized as follows: we consider given two point patterns (sets of points) $\boldsymbol{X} = \{\boldsymbol{a}_1, \boldsymbol{a}_2, \cdots, \boldsymbol{a}_{|P|}\}$ and $\boldsymbol{Y} = \{\boldsymbol{b}_1, \boldsymbol{b}_2, \cdots, \boldsymbol{b}_{|Q|}\}$ in 3-D space, and we want to find the similarity transformation parameters ($\boldsymbol{R}$:rotation, $\boldsymbol{t}$:translation, $c$:scaling) giving the minimum value of the RMSE (root mean squared error) $e(\boldsymbol{R}, \boldsymbol{t}, c)$ of these two point patterns,

$$e(\boldsymbol{R}, \boldsymbol{t}, c) = \frac{1}{|P|}\frac{1}{|Q|}\sum_{p=1}^{|P|}\sum_{q=1}^{|Q|}\min_{p\in P, q\in Q}\|\boldsymbol{a}_p - (c\boldsymbol{R}\boldsymbol{b}_q + \boldsymbol{t})\|, \quad (1)$$

where $P = \{1, 2, \cdots, |P|\}$ and $Q = \{1, 2, \cdots, |Q|\}$ are sets of indices of data point, and $|P| \neq |Q|$. In order to solve this problem, the ICP (Iterative Closest Point) algorithm [3] has been proposed. This algorithm performs matching of the memorized (or template) and the measured datasets and estimates parameters of 3-D coordinates transformation by a gradient method which minimizes RMSE. However, in ICP algorithm, a deterioration of resolution according to the measured distance of actual range sensor, the lack of data points, etc. are not taken into consideration. On the other hand, Nagao, et al. [4] have proposed a method for reduction of influence of the deterioration of resolution for the actual LRF datasets. However, this method needs many preprocessings for the measured data and the adjustment of parameters. Furthermore, from the point of view of recognition ability of human being, there are researches for abstraction and recognition of 2-D and/or 3-D data using artificial neural networks [5], [6]. However, these have tackled by the appearance based approach, and have not used the 3-D datasets for data matching directly. Therefore, we propose a method of estimating the 3-D affine transformation parameters between the template and the measured data sets at high speed and stably using the result of SVD (singular value decomposition) analysis of them. Further, we propose the robust matching method of the datasets which have difference resolutions. Moreover, through numerical simulations and experiments, we demonstrate that our method is able to achieve stable and robust recognition for actual measured datasets of LRF.

## 2. 3-D MATCHING USING SVD

### Invariance of SVD for 3-D Rotation

Let $\boldsymbol{A} = \left(\boldsymbol{a}_1, \cdots, \boldsymbol{a}_p, \cdots, \boldsymbol{a}_{|P|}\right)^T \in \mathbb{R}^{|P|\times 3}$ be a matrix consisting of the points $\boldsymbol{a}_p \in \boldsymbol{X}$ in 3-D space, and let $\hat{\boldsymbol{A}} \triangleq \boldsymbol{A}\boldsymbol{R}^T$ be its rotated matrix where the rotation matrix $\boldsymbol{R} \triangleq \boldsymbol{R}(\theta_x)\boldsymbol{R}(\theta_y)\boldsymbol{R}(\theta_z)$ defined by the rotation angle $\theta_x$ (resp. $\theta_y$, $\theta_z$) around the $x$-axis (resp. $y$-axis, $z$-axis).

Now we show that the results of SVD of these matrices have invariance to the 3-D rotation. First, the SVD of the matrix $\boldsymbol{A}$ and the matrix $\hat{\boldsymbol{A}}$ are

$$\boldsymbol{A} = \boldsymbol{U}\boldsymbol{D}\boldsymbol{V}^T, \quad (2)$$

$$\hat{\boldsymbol{A}} = \hat{\boldsymbol{U}}\hat{\boldsymbol{D}}\hat{\boldsymbol{V}}^T, \quad (3)$$

where the left singular matrices are $\boldsymbol{U}, \hat{\boldsymbol{U}} \in \mathbb{R}^{L\times 3}$, the right singular matrices are $\boldsymbol{V}, \hat{\boldsymbol{V}} \in \mathbb{R}^{3\times 3}$, and the singular matrices are

$$\boldsymbol{D} = \mathrm{diag}(d_1, d_2, d_3) \in \mathbb{R}^{3\times 3}, \ (d_1 \geq d_2 \geq d_3 \geq 0), \quad (4)$$

$$\hat{\boldsymbol{D}} = \mathrm{diag}(\hat{d}_1, \hat{d}_2, \hat{d}_3) \in \mathbb{R}^{3\times 3}, \ (\hat{d}_1 \geq \hat{d}_2 \geq \hat{d}_3 \geq 0). \quad (5)$$

Since $\boldsymbol{R}$ is orthogonal,

$$\hat{\boldsymbol{A}}\hat{\boldsymbol{A}}^T = \boldsymbol{A}\boldsymbol{R}^T\boldsymbol{R}\boldsymbol{A}^T = \boldsymbol{A}\boldsymbol{A}^T. \quad (6)$$

On the other hand,

$$\boldsymbol{A}\boldsymbol{A}^T = \boldsymbol{U}\boldsymbol{D}^2\boldsymbol{U}^T, \quad (7)$$

$$\hat{\boldsymbol{A}}\hat{\boldsymbol{A}}^T = \hat{\boldsymbol{U}}\hat{\boldsymbol{D}}^2\hat{\boldsymbol{U}}^T. \quad (8)$$

Thus, from Eq.(6)-(8),

$$\boldsymbol{D} = \hat{\boldsymbol{D}}, \quad (9)$$

$$\boldsymbol{U} = \hat{\boldsymbol{U}}, \quad (10)$$

are obtained [7], [8]. Namely, the left singular matrix and the singular matrix are invariant to 3-D rotation. Therefore, only the right singular matrix is transformed by the rotation matrix as follows,

$$\boldsymbol{R}\boldsymbol{V} = \hat{\boldsymbol{V}}. \quad (11)$$

Moreover, since $\boldsymbol{V}$ is orthogonal, the rotation matrix $\boldsymbol{R}$ is calculated by

$$\hat{\boldsymbol{V}}\boldsymbol{S}\boldsymbol{V}^T = \boldsymbol{R}\boldsymbol{V}\boldsymbol{S}\boldsymbol{V}^T = \boldsymbol{R}, \quad (12)$$

where

$$\boldsymbol{S} = \begin{cases} \boldsymbol{I} & \text{if } \det\left(\hat{\boldsymbol{V}}\right)\det\left(\boldsymbol{V}\right) = 1, \\ \mathrm{diag}(1, \cdots, 1, -1) & \text{if } \det\left(\hat{\boldsymbol{V}}\right)\det\left(\boldsymbol{V}\right) = -1. \end{cases} \quad (13)$$

This matrix $\boldsymbol{S}$ was introduced by Umeyama[9] in order to prevent the reflection matching.

**Estimation of Rotation Matrix**

Next, we consider the matching of the template data matrix $\tilde{\boldsymbol{C}} = \left(\tilde{\boldsymbol{c}}_1, \cdots, \tilde{\boldsymbol{c}}_{|P|}\right)^T$ and the actual range data matrix $\tilde{\boldsymbol{C}}' = \left(\tilde{\boldsymbol{c}}'_1, \cdots, \tilde{\boldsymbol{c}}'_{|Q|}\right)^T$ obtained by the LRF, where $|P| \neq |Q|$ and these are without correspondence. Here, we define matrices $\bar{\boldsymbol{C}}$ and $\bar{\boldsymbol{C}}'$ consisting of the mean vector of $\tilde{\boldsymbol{C}}$ and $\tilde{\boldsymbol{C}}'$, and variances as follows:

$$\bar{\boldsymbol{C}} \triangleq (\boldsymbol{\mu}_C, \cdots, \boldsymbol{\mu}_C)^T \in \mathbb{R}^{|P|\times 3}, \quad (14)$$

$$\bar{\boldsymbol{C}}' \triangleq (\boldsymbol{\mu}_{C'}, \cdots, \boldsymbol{\mu}_{C'})^T \in \mathbb{R}^{|Q|\times 3}, \quad (15)$$

$$\boldsymbol{\mu}_C \triangleq \frac{1}{|P|}\sum_{p=1}^{|P|}\tilde{\boldsymbol{c}}_p, \quad (16)$$

$$\boldsymbol{\mu}_{C'} \triangleq \frac{1}{|Q|}\sum_{q=1}^{|Q|}\tilde{\boldsymbol{c}}'_q, \quad (17)$$

$$\sigma_C^2 \triangleq \frac{1}{|P|}\sum_{p=1}^{|P|}\|\boldsymbol{c}_p - \boldsymbol{\mu}_C\|^2, \quad (18)$$

$$\sigma_{C'}^2 \triangleq \frac{1}{|Q|}\sum_{q=1}^{|Q|}\|\boldsymbol{c}'_q - \boldsymbol{\mu}_{C'}\|^2. \quad (19)$$

Further, we obtain the normalized matrices about translation and scaling by

$$\boldsymbol{C} \triangleq \left(\tilde{\boldsymbol{C}} - \bar{\boldsymbol{C}}\right)/\sigma_C^2 = \left(\boldsymbol{c}_1, \cdots, \boldsymbol{c}_{|P|}\right), \quad (20)$$

$$\boldsymbol{C}' \triangleq \left(\tilde{\boldsymbol{C}}' - \bar{\boldsymbol{C}}'\right)/\sigma_{C'}^2 = \left(\boldsymbol{c}'_1, \cdots, \boldsymbol{c}'_{|Q|}\right). \quad (21)$$

When the covariance matrices of $\boldsymbol{C}$ and $\boldsymbol{C}'$ given by,

$$\boldsymbol{W} \triangleq \boldsymbol{C}^T\boldsymbol{C} = \sum_{p=1}^{|P|}\boldsymbol{c}_p\boldsymbol{c}_p^T, \quad (22)$$

$$\boldsymbol{W}' \triangleq \boldsymbol{C}'^T\boldsymbol{C}' = \sum_{q=1}^{|Q|}\boldsymbol{c}'_q\boldsymbol{c}'^T_q, \quad (23)$$

are almost same, namely $\boldsymbol{W} \simeq \boldsymbol{W}'$, we have

$$\boldsymbol{V}_{C'} \simeq \boldsymbol{V}_C, \quad (24)$$

$$\boldsymbol{D}_{C'} \simeq \boldsymbol{D}_C, \quad (25)$$

where

$$\boldsymbol{C} = \boldsymbol{U}_C\boldsymbol{D}_C\boldsymbol{V}_C^T, \quad (26)$$

$$\boldsymbol{C}' = \boldsymbol{U}_{C'}\boldsymbol{D}_{C'}\boldsymbol{V}_{C'}^T, \quad (27)$$

and

$$\boldsymbol{W} = \boldsymbol{V}_C\boldsymbol{D}_C^2\boldsymbol{V}_C^T, \quad (28)$$

$$\boldsymbol{W}' = \boldsymbol{V}_{C'}\boldsymbol{D}_{C'}^2\boldsymbol{V}_{C'}^T. \quad (29)$$

Then the rotation matrix of $\boldsymbol{C}'' \triangleq \boldsymbol{C}'\boldsymbol{R}^T$ is able to estimate as follows,

$$\boldsymbol{V}_{C''}\boldsymbol{V}_C^T = \left(\boldsymbol{R}\boldsymbol{V}_{C'}\right)\boldsymbol{V}_C^T \simeq \left(\check{\boldsymbol{R}}\boldsymbol{V}_C\right)\boldsymbol{V}_C^T = \check{\boldsymbol{R}}, \quad (30)$$

where

$$\boldsymbol{C}'' \triangleq \boldsymbol{C}'\boldsymbol{R}^T = \boldsymbol{U}_{C'}\boldsymbol{D}_{C'}\left(\boldsymbol{R}\boldsymbol{V}_{C'}\right)^T = \boldsymbol{U}_{C'}\boldsymbol{D}_{C'}\boldsymbol{V}_{C''}^T. \quad (31)$$

In this research, we call $\check{\boldsymbol{R}}$ the estimated rotation matrix.

**Data Matching Algorithm**

First, the $n$th template pattern

$$\boldsymbol{A}^{(n)} = \left(\boldsymbol{a}_1^{(n)}, \cdots, \boldsymbol{a}_p^{(n)}, \cdots, \boldsymbol{a}_{|P|}^{(n)}\right)^T \in \mathbb{R}^{|P|\times 3} \quad (32)$$

is generated in advance, where $n \in N = \{1, \cdots, |N|\}$. These patterns are generated from CAD (computer-aided-design) model or actual measured data points, and are generated so that the mean vector and the variance of them should be as follows:

$$\boldsymbol{\mu}_{A^{(n)}} = \frac{1}{|P|}\sum_{p=1}^{|P|}\boldsymbol{a}_p^{(n)} = 0, \quad (33)$$

$$\sigma_{A^{(n)}}^2 = \frac{1}{|P|}\sum_{p=1}^{|P|}\left\|\boldsymbol{a}_p^{(n)} - \boldsymbol{\mu}_{A^{(n)}}\right\|^2 = 1. \quad (34)$$

Moreover, the SVD

$$\boldsymbol{A}^{(n)} = \boldsymbol{U}_{A^{(n)}}\boldsymbol{D}_{A^{(n)}}\boldsymbol{V}_{A^{(n)}}^T, \quad (35)$$

are calculated and $\boldsymbol{V}_{A^{(n)}}$ is registered.

Next, the matrix of measured points of the target object is generated as follows:

$$\begin{aligned}\tilde{\boldsymbol{B}}^{(m)} &= \left( \begin{array}{ccccc} \tilde{\boldsymbol{b}}_1^{(m)} & \cdots & \tilde{\boldsymbol{b}}_q^{(m)} & \cdots & \tilde{\boldsymbol{b}}_{|Q|}^{(m)} \end{array} \right)^T \\ &= \left( \begin{array}{ccccc} \tilde{b}_{1x}^{(m)} & \cdots & \tilde{b}_{qx}^{(m)} & \cdots & \tilde{b}_{|Q|x}^{(m)} \\ \tilde{b}_{1y}^{(m)} & \cdots & \tilde{b}_{qy}^{(m)} & \cdots & \tilde{b}_{|Q|y}^{(m)} \\ \tilde{b}_{1z}^{(m)} & \cdots & \tilde{b}_{qz}^{(m)} & \cdots & \tilde{b}_{|Q|z}^{(m)} \end{array} \right)^T \end{aligned} \quad (36)$$

where $m \in M = \{1, 2, \cdots, |M|\}$ is index of the measured pattern. Then this matrix is normalized by using the mean vector and the variance of elements as follows,

$$\begin{aligned}\boldsymbol{B}^{(m)} &= \left( \tilde{\boldsymbol{B}}^{(m)} - \bar{\boldsymbol{B}}^{(m)} \right) / \sigma_{B^{(m)}}^2 \\ &= \left( \boldsymbol{b}_1^{(m)}, \boldsymbol{b}_2^{(m)}, \cdots, \boldsymbol{b}_j^{(m)} \right)^T . \end{aligned} \quad (37)$$

Here, since the infrared rays irradiated by the LRF are not uniformly distributed on a target object depending on change of the conditions to measure, the mean vector of the measured pattern is calculate by means of the maximum and the minimum value of elements of the matrix as follows,

$$\bar{\boldsymbol{B}}^{(m)} = \left( \boldsymbol{\mu}_{B^{(m)}}, \cdots, \boldsymbol{\mu}_{B^{(m)}} \right)^T \in \mathbb{R}^{|Q| \times 3}, \quad (38)$$

$$\boldsymbol{\mu}_{B^{(m)}} = \frac{1}{2} \left( \begin{array}{c} \max\limits_{q \in Q} \{\tilde{b}_{qx}\} + \min\limits_{q \in Q} \{\tilde{b}_{qx}\} \\ \max\limits_{q \in Q} \{\tilde{b}_{qy}\} + \min\limits_{q \in Q} \{\tilde{b}_{qy}\} \\ \max\limits_{q \in Q} \{\tilde{b}_{qz}\} + \min\limits_{q \in Q} \{\tilde{b}_{qz}\} \end{array} \right), \quad (39)$$

$$\sigma_{B^{(m)}}^2 = \frac{1}{|Q|} \sum_{q=1}^{|Q|} \left\| \boldsymbol{b}_q^{(m)} - \boldsymbol{\mu}_{B^{(m)}} \right\|^2 . \quad (40)$$

Next,

$$\boldsymbol{B}^{(m)} = \boldsymbol{U}_{B^{(m)}} \boldsymbol{D}_{B^{(m)}} \boldsymbol{V}_{B^{(m)}}^T \quad (41)$$

is calculated and the estimated rotation matrix between $\boldsymbol{A}^{(n)}$ and $\boldsymbol{B}^{(m)}$ is derived by using the right singular matrices of Eq.(35) and Eq.(41) as follows,

$$\check{\boldsymbol{R}}^{(nm)} = \boldsymbol{V}_{B^{(m)}} \boldsymbol{S} \boldsymbol{V}_{A^{(n)}}^T , \quad (42)$$

where $\boldsymbol{S}$ is calculated by Eq.(13). Further, the inverse rotation pattern of $\boldsymbol{B}^{(m)}$ is calculated by using this estimated rotation matrix as follows,

$$\begin{aligned}\check{\boldsymbol{B}}^{(nm)} &= \boldsymbol{B}^{(m)} \check{\boldsymbol{R}}^{(nm)} \\ &= \left( \check{\boldsymbol{b}}_1^{(nm)}, \check{\boldsymbol{b}}_2^{(nm)}, \cdots, \check{\boldsymbol{b}}_j^{(nm)} \right)^T . \end{aligned} \quad (43)$$

At last, the best matching $\varepsilon$th template pattern for $m$th measured pattern is decided by

$$\varepsilon = \underset{n \in N}{\operatorname{argmin}} \left( \frac{1}{|P|} \frac{1}{|Q|} \sum_{p=1}^{|P|} \sum_{q=1}^{|Q|} \min_{p \in P, q \in Q} \left\| \boldsymbol{a}_p^{(n)} - \check{\boldsymbol{b}}_q^{(nm)} \right\| \right) . \quad (44)$$

Since this algorithm performs the matching between the template and the measured patterns at once using the estimated rotation matrices, the matching result can be obtained with high speed and stability.

## 3. NUMERICAL SIMULATION

Here, the validity of the 3-D object recognition method proposed in this research is estimated by the numerical simulations.

### Test Patterns

The template and the test patterns are shown in Fig.1(a)-(d). The template pattern shown in Fig.1(a) is a right isosceles triangle consisting of 4995 data points, and the one of its vertex was cut so that the result of SVD is stable. Moreover, Fig.1(b) and (d) are a rectangle and a circle consisting of 9829 and 7663 points, respectively, and those parts were cut for the same reason. Especially, the #2 test pattern shown in Fig.1(c) was made of the template pattern by rotating 60 degrees around each axis. Furthermore, in order not to make the 3rd singular value not small, these patterns were generated by giving a certain value at random in the direction perpendicular to the plane.

### Result of Simulations

The rotation matrix used for generating the #2 test pattern from the template pattern was

$$\boldsymbol{R} = \left( \begin{array}{ccc} 0.250 & -0.058 & 0.966 \\ 0.433 & 0.899 & -0.058 \\ -0.866 & 0.433 & 0.250 \end{array} \right), \quad (45)$$

and the estimated rotation matrices between the template and the test patterns were

$$\check{\boldsymbol{R}}^{(11)} = \left( \begin{array}{ccc} 0.139 & -0.216 & 0.967 \\ 0.937 & 0.344 & -0.058 \\ -0.320 & 0.914 & 0.250 \end{array} \right), \quad (46)$$

$$\check{\boldsymbol{R}}^{(12)} = \left( \begin{array}{ccc} 0.250 & -0.058 & 0.967 \\ 0.433 & 0.899 & -0.058 \\ -0.866 & 0.433 & 0.250 \end{array} \right), \quad (47)$$

$$\check{\boldsymbol{R}}^{(13)} = \left( \begin{array}{ccc} 0.248 & -0.065 & 0.967 \\ 0.458 & 0.886 & -0.058 \\ -0.853 & 0.457 & 0.250 \end{array} \right). \quad (48)$$

Moreover, the test patterns rotated by using the above rotation matrices are shown in Fig.2(a)-(c). First, it was found from Eq.(45) and Eq.(47) that the rotation matrix between congruent patterns was estimated correctly. Further, it was found from Fig.1(b) and (d) that the rotation matrices between the patterns which have different shapes were also estimated appropriately. Next, the RMSE between the template and the test patterns are shown in Tab.I. It was found from the result that the estimation of 3-D coordinates transformation and 3-D pattern matching could be achieve correctly by the proposed method.

## 4. EXPERIMENT

In this section, we demonstrate the ability of the proposed method for the actual measured points without correspondence.

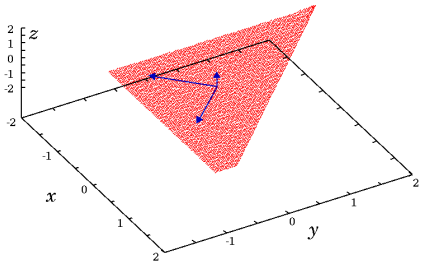


(a) Template pattern.

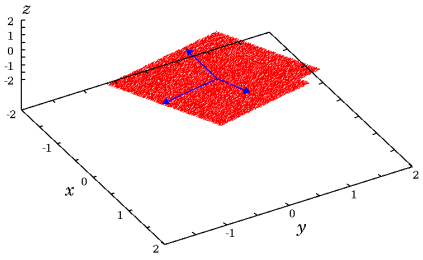


(b) Test pattern #1.

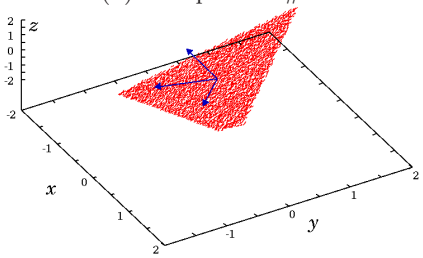


(c) Test pattern #2.

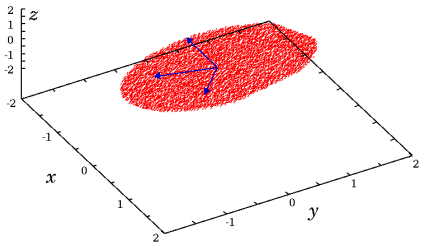


(d) Test pattern #3.

Fig. 1. A template and test patterns. The arrows represent the orientation of the singular vectors.

TABLE I
Matching result of the numerical simulations.

| Test pattern | #1 | #2 | #3 |
|---|---|---|---|
| RMSE | 0.118 | 0.000 | 0.149 |

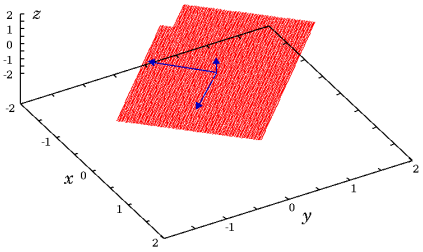


(a) Rotated test pattern #1.

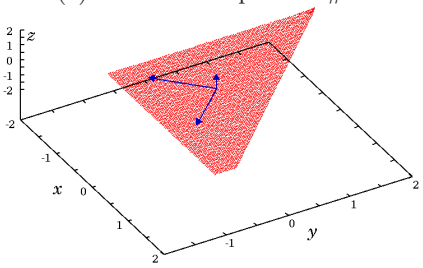


(b) Rotated test pattern #2.

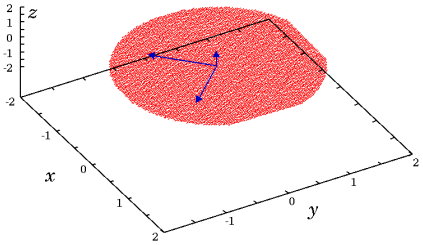


(c) Rotated test pattern #3.

Fig. 2. Rotated test patterns. The arrows represent the orientation of the singular vectors.

### Measurement of 3-D Object by LRF

We used the LRF (LMS200 from SICK, Inc.) which basically scans the horizontal 2D plane to measure the distance to the object, where the maximum measure distance is 8191[mm], and the maximum scanning range is 180[deg] with angular resolution 0.25[deg]. In order to scan 3-D space, we have designed to make of a suspension unit [1], [2] for rotating the LRF vertically by means of a geared stepping motor with angle resolution 0.05[deg]. Thus, we can obtain the 3-D position $\boldsymbol{x}_{ij}$ from the measured distance $d_{ij}$ for the horizontal angle $\theta_i$ and the vertical rotation angle $\phi_j$ as follows,

$$\boldsymbol{x}_{ij} = \begin{pmatrix} d_{ij}\cos\phi_j\cos\theta_i \\ d_{ij}\sin\phi_j \\ d_{ij}\cos\phi_j\sin\theta_i \end{pmatrix} = \begin{pmatrix} x_{ij} \\ y_{ij} \\ z_{ij} \end{pmatrix} \tag{49}$$

where we use the angles given by

$$\theta_i = 0.25i + \theta_0 \quad (i = 0, 1, \cdots, 400) \tag{50}$$

$$\phi_j = 0.25j + \phi_0 \quad (j = 0, 1, \cdots, 400) \tag{51}$$

where $\theta_0 = 40$[deg] (resp. $\phi_0 = -40$[deg]) is the starting horizontal (resp. vertical) scanning angle. Then by using these measured points, the 3-D dataset

$$\boldsymbol{X}_a = \{\boldsymbol{x}_{ij}\} \tag{52}$$

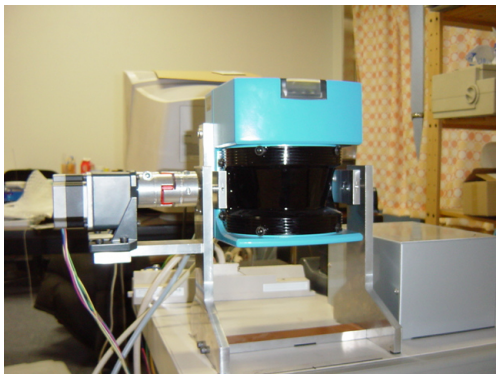

Fig. 3. LRF and suspension unit.

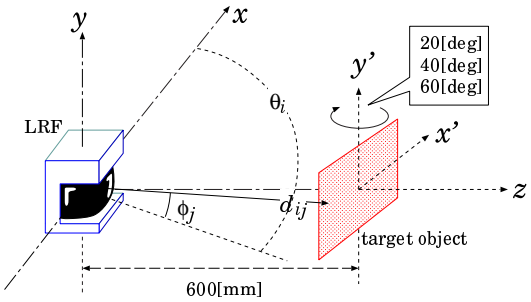


Fig. 4. LRF coordinate system.

was obtained, and the measured pattern was generated as follows,

$$\tilde{\boldsymbol{B}} = \left(\boldsymbol{b}_1, \cdots, \boldsymbol{b}_q, \cdots, \boldsymbol{b}_{|Q|}\right)^T, \boldsymbol{b}_q \in \boldsymbol{X}_a, \tag{53}$$

where the point $\boldsymbol{b}_q$ was the measured point on the target object.

### Template and Measured Datasets

Fig.5(a) shows the one of the template pattern and Fig.5(b)-(d) show the measured patterns of 70[mm]×45[mm] rectangle papers which were set 600[mm] ahead of the LRF, and were rotated 20[deg], 40[deg], and 60[deg] around y-axis, respectively (see Fig.4). Moreover, these test patterns were already normalized by Eq.(37). Furthermore, we prepared the two more template patterns, i.e., the right isosceles triangle and the circle template patterns used in the above numerical simulations besides the rectangle template pattern.

### Result of Experiments

The estimated rotation matrices between the template and the measured patterns were calculated, and the measured patterns were rotated by these estimated rotation matrices. The rotated measured patterns which correspond to the rectangle template pattern are shown in Fig.6(a)-(c). These results show that each principal components of the patterns corresponded with that of

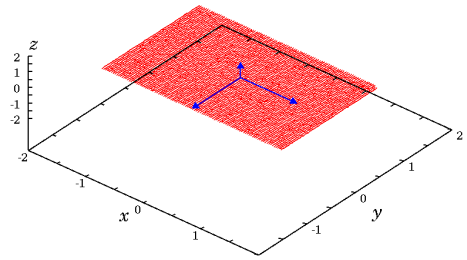

(a) Rectangle template pattern (9996 points).

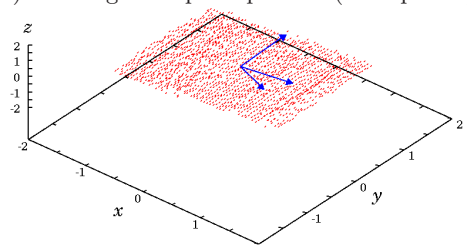

(b) Measured pattern of the object rotated 20[deg] (1792 points).

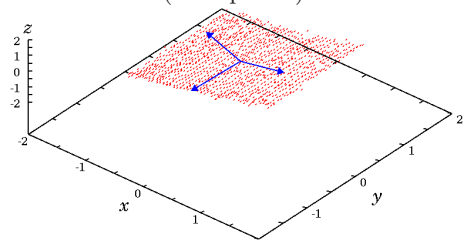

(c) Measured pattern of the object rotated 40[deg] (1288 points).

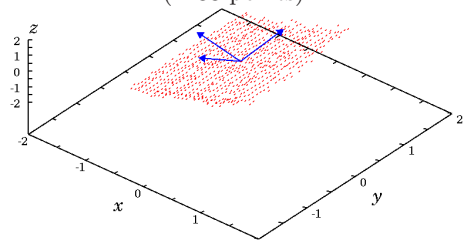

(d) Measured pattern of the object rotated 60[deg] (777 points).

Fig. 5. Measured patterns. The arrows represent the orientation of the singular vectors.

the template pattern appropriately. Next, the matching resuts between the template pattern and these measured patterns are shown in Tab.II. It was found from these results that the RMSE of the rectangle template pattern and the measured patterns were minimum for all rotated angle, so that the shape of the measured patterns had been discriminated correctly. Moreover, since the number of the measuring point on the object decreases as the inclination to the LRF of the object becomes large, there is a tendency for discernment of the shape of the measured patterns to become difficult.

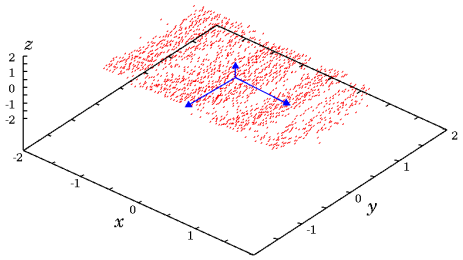


(a) Rotated measured pattern of the 20[deg] rotated object.

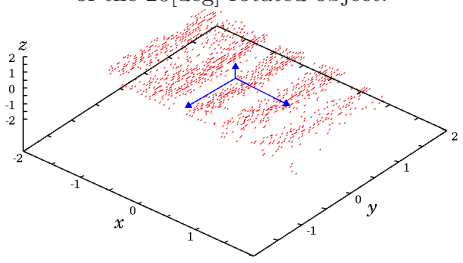


(b) Rotated measured pattern of the 40[deg] rotated object.

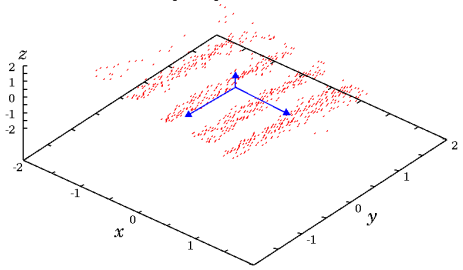


(c) Rotated measured pattern of the 60[deg] rotated object.

Fig. 6. Rotated measured patterns. The arrows represent the orientation of the singular vectors.

## 5. CONCLUDING REMARKS

We have presented the 3-D data matching method. As the results of the numerical simulations and the experiments, we could find the parameters of 3-D affine transformation which match the registered template patterns to the measured patterns appropriately, and could discriminate the shape of patterns by the presented method. Furthermore, there is problem which we would like to tackle, such as the construction of the neural network model associates the recognition system of human being and the presented method. As future work, the application of the presented method to recognition of the object which consists of plural planes and curved surfaces can be considered. On the other hand, for the actual application of this method, the data processing algorithm for data extraction of the target object from measured datasets is also required.

TABLE II

Matching result of the experiments. The values represent the RMSE between each template and test patterns.

| Measured pattern | 20[deg] | 40[deg] | 60[deg] |
|---|---|---|---|
| Rectangle | 0.174 | 0.185 | 0.234 |
| Triangle | 0.243 | 0.258 | 0.300 |
| Circle | 0.229 | 0.233 | 0.252 |

## References


[1] H. Surmann, K. Lingemann, A. Nüchter and J. Hertzberg, "A 3D laser range finder for autonomous mobile robots, " *Proc. of the 32nd ISR*, pp. 153–158, 2001.

[2] H. Surmann, K. Lingemann, A. Nüchter and J. Hertzberg, "Fast acquiring and analysis of three dimensional laser range data," *Proc. of VMV 2001*, pp.59–66, 2001.

[3] P. J. Besl and N. D. McKay, "A Method for Registration of 3-D Shapes," *IEEE Trans. on Pattern Analysis and Machine Intelligence*, Vol. 14, No. 2, pp. 239–256, 1992.

[4] K. Nagao, T. O and K. Deguchi, "Range Image Matching for Object Recognition in Real Scene," *Trans. SICE (in Japanese)*, Vol. 40, No. 1, pp. 10–17, 2004.

[5] N. Intrator, J. I. Gold, H. H. Bülthoff and S.Edelman, "3D Object Recognition Using Unsupervised Feature Extraction," *Proc. of NIPS 1991*, pp. 460–467, 1991.

[6] S. Kurogi, T. Nishida and K. Yamamoto, "Image Transformation of Local Features for Rotation Invariant Pattern Matching," *Proc. of ICONIP 2001*, pp. 693–698, 2001.

[7] L. Mirsky, "Symmetric gage functions and unitarily invariant norms," *Quarterly Journal of Mathematics*, No. 11, pp. 50–59, 1960.

[8] G. H. Golub, A. Hoffman and G. W. Stewart, "A generalization of the Eckart-Young-Mirsky Matrix Approximation Theorem," *Linear Algebra and Applications*, No. 88/89, pp. 317–327, 1987.

[9] S. Umeyama, "Least-Squares Estimation of Transformation Parameters Between Two Point Patterns," *IEEE Trans. on Pattern Analysis and Machine Intelligence*, Vol. 13, No. 4, pp. 376–380, 1991.